

Direct synthesis of all-inorganic heterostructure CdSe/CdS QDs in aqueous solution for improved photocatalytic hydrogen generation

Zhi-Jun Li,^{†,#} Xiang-Bing Fan,^{†,#} Xu-Bing Li,[†] Jia-Xin Li,[†] Fei Zhan,[‡] Ye Tao,^{*,‡}
Xiaoyi Zhang,[§] Qing-Yu Kong,[‡] Ning-Jiu Zhao,[&] Jian-Ping Zhang,[&] Chen Ye,[†]
Yu-Ji Gao,[†] Xu-Zhe Wang,[†] Qing-Yuan Meng,[†] Ke Feng,[†] Bin Chen,[†] Chen-Ho
Tung,[†] Li-Zhu Wu^{*,†}

[†]Key Laboratory of Photochemical Conversion and Optoelectronic Materials, Technical Institute of Physics and Chemistry, Chinese Academy of Sciences, Beijing 100190, P. R. China

[‡]Beijing Synchrotron Radiation Facility, Institute of High Energy Physics, Chinese Academy of Sciences, Beijing 100049, P. R. China

[§]X-ray Sciences Division, Advanced Photon Source, Argonne National Laboratory, 9700 South Cass Avenue, Argonne, IL 60430, USA

[‡]Synchrotron SOLEIL, L'Orme des Merisiers, St.Aubin 91192 GIF-sur-YVETTE CEDEX, France

[&]Department of Chemistry, Renmin University of China, Beijing 100872, P. R. China

Corresponding Author

*Address correspondence to lzwu@mail.ipc.ac.cn and taoy@ihep.ac.cn

Author Contributions

These authors contributed equally.

Table of Contents

1. Instruments for characterization.
2. Synthesis and characterization of water-soluble MPA-CdSe QDs.
3. Control experiment of SILAR method for the synthesis.
4. Steady state and time-resolved emission spectroscopy measurement.
5. Femtosecond transient absorption spectroscopy measurement.
6. Steady state and time-resolved X-ray transient absorption (XTA) measurement.
7. XPS sensitivity calibration and surface composition calculation.
8. The wt.% composition of the CdSe QDs and the CdSe/CdS QDs determined by ICP-OES measurement.
9. The internal quantum efficiency (IQE) determination.
10. The turnover number (TON) determination.
11. Measured and estimated time constants of recovery kinetics of emission delay.
12. The kinetics of the excited QD population ($N_{QD^*}(t)$)
13. Figure S1. The corresponding lattice spacing along the crystalline (111) directions of the zinc blende lattice in CdSe/CdS QDs.
14. Figure S2-S5. Control experiments of synthesis by typical SILAR method.
15. Figure S6. ^1H NMR spectra of MPA obtained from CdSe QDs and the CdSe/CdS QDs.
16. Figure S7. FT-IR spectra of MPA-CdSe QDs and CdSe/CdS QDs.
17. Figure S8. XRD data of Ni 2p signals of the CdSe/CdS QDs and CdSe/CdS-Ni(OH)₂ photocatalyst.
18. Figure S9. Comparison of photocatalytic H₂-production performance of as-prepared CdSe/CdS QDs with CdSe/CdS QDs prepared by organometallic route.
19. Figure S10. Photocatalytic H₂ evolution from the systems with varied components and condition.
20. Figure S11. Photocatalytic H₂ evolution with various concentrations of NiCl₂·6H₂O.
21. Figure S12. Energy structure and cyclic voltammetry properties of QDs.
22. Figure S13. The femtosecond TA spectra of CdSe/CdS QDs in the absence and presence of Ni(II).
23. Figure S14. The femtosecond TA kinetics of CdSe QDs and CdSe QDs/Ni(II) at 430 nm.
24. References.

1. Instruments for characterization.

UV-vis absorption spectra were recorded with a Shimadzu 1601-PC spectrophotometer. The Raman spectrum was recorded with a Via-Reflex Raman system, by using a 785 nm excitation wavelength. Attenuated total reflectance FT-IR spectra were taken on Excalibur 3100 system (Varian, USA). HRTEM was performed by JEM 2100F (operated at an accelerating voltage of 200 kV). XRD spectra were taken on a Bruker D8 Focus under Cu-K α radiation at ($\lambda = 1.54056 \text{ \AA}$). The XPS measurements were performed on an ESCALAB 250 spectrophotometer with Al-K α radiation. The binding energy scale was calibrated using the C 1s peak at 284.6 eV. ^1H NMR spectra were recorded using a Bruker Avance DPX 400 MHz instrument with deuterium oxide as solvent. The zeta potential was measured using a Malvern Zetasizer 3000HS. Cyclic voltammetry experiments were performed in a one-compartment three electrode cell, using glassy carbon working electrode, platinum counter electrode and SCE as reference electrode under nitrogen. All pH measurements were made with a Model pHs-3C meter (Mettler Toledo FE20, China). Gas chromatography (GC) was performed by Techcomp 7890 II GC using a 5 \AA molecular sieve column, thermal conductivity detector. The composition of QDs was determined by Inductively Coupled Plasma Optical Emission Spectrometry (ICP-OES, Varian 710-OES, USA).

2. Synthesis and characterization of water-soluble MPA-CdSe QDs.

2.1. Preparation of Na₂SeSO₃ solution.

Briefly,¹ 40 mg selenium powder was transferred to 100 mL Na₂SO₃ (189 mg) water solution. The resulting mixture solution was then heated to $\sim 100^\circ\text{C}$ and refluxed until the selenium powder dissolved and obtained transparent Na₂SeSO₃ solution.

2.2. Synthesis of water-soluble MPA-CdSe QDs.

An aqueous colloidal MPA-CdSe QDs solution was prepared by the reaction between Cd²⁺ and Na₂SeSO₃ solution following the method described as follows:¹ Cd²⁺ precursor solution was prepared by mixing a solution of CdCl₂·2.5H₂O and stabilizer (MPA) solution, and adjusted pH to 11 with 1 M NaOH. The typical molar ratio of Cd:MPA:Se was 1:1.5:0.25 in the experiment. This solution was placed in a three-necked flask, fitted and de-aerated with N₂ bubbling for 30 min. Finally, the solution was heated and refluxed for about 3.0 h to promote the growth of CdSe QDs.

2.3. The size and extinction coefficient (ϵ) of MPA-CdSe QDs.

According to the work of Peng and coworkers,² the diameter (**D**) and extinction coefficient (ϵ) of the MPA-CdSe QDs can be determined by the equations as follows:

$$D = (1.6122 \times 10^{-9})\lambda^4 - (2.6575 \times 10^{-6})\lambda^3 + (1.6242 \times 10^{-3})\lambda^2 - (0.4277)\lambda + 41.57 \quad (1)$$

$$\epsilon = 5857(D)^{2.65} \quad (2)$$

Where **D** (nm) is the diameter or size of a given nanocrystal sample, λ is the wavelength of the first absorption peak (from low energy, at 430 nm) of the corresponding sample and ϵ is the extinction coefficient of the corresponding sample. In our experiments, the diameter (**D**) of the MPA-CdSe QDs was determined as 1.9 nm and the extinction coefficient ϵ was 3.2×10^4 (L mol⁻¹ cm⁻¹) according to equation (1) and (2), respectively. The concentration of the MPA-CdSe QDs was determined as 2×10^{-5} M using the Beer–Lambert law.

2.4. The optical and theoretical calculation of band gap (E_g^{op} , E_g^{th}) for CdSe QDs

The most important consequence of the quantum confinement effect is the size dependence of the band gap. By confining the exciton of a QD, the band gap may be tuned to a precise energy depending on the dimensionality and degree of confinement.^{3, 4} The optical band gap (E_g^{op}) of QDs could be calculated from the intersection of the absorption and emission spectra (λ_{0-0}) of the corresponding sample using equation (3);⁵ the other way to theoretically calculate the band gap (E_g^{th}) is based on the diameter of the corresponding sample using equation (4).^{6,}

7

$$E_g^{op} = \frac{1240}{\lambda_{0-0}} \quad (3)$$

$$E_g^{th} = E_g^b + \frac{h}{8D^2} \left(\frac{1}{m_e} + \frac{1}{m_h} \right) \quad (4)$$

Herein, E_g^{op} and E_g^{th} (eV) is optical and theoretical band gap of QDs, λ_{0-0} (nm) the intersection of the absorption and emission spectra of corresponding sample, E_g^b (for bulk CdSe, $E_g^b = 1.7$ eV, $E_{cb}^b = -0.6$ V, $E_{vb}^b = 1.1$ V vs NHE)^{8, 9} is the band gap of the corresponding bulk sample, h is Planck's constant, D is the diameter of QDs, and m_e ($0.13 m_0$, $m_0 = 9.1095 \times 10^{-31}$ kg) and m_h ($0.44 m_0$) are the effective masses of electrons and holes, respectively. m_0 is the mass of free electrons.

In our experiments, the intersection of the absorption and emission spectra (λ_{0-0}) of CdSe QDs was 460 nm (Figure S11a), E_g^{op} was determined as 2.7 eV from equation (3). Alternatively, based on the diameter (**D**) of CdSe QDs (1.9 nm), the corresponding E_g^{th} was determined as 2.7 eV from equation (4), consistent with the result from

equation (3). Although CdSe QDs used in this study have larger band gap, the relative positions of valence band are likely to be close to the bulk value, and most of the band gap increase is reflected in the shift of conduction band to more negative potentials.⁴ This is because of the higher degeneracy and closely spaced energy levels in the valence band, and the holes effective mass m_h is larger than the electron mass m_e in CdSe.¹⁰

2.5. Structural Characterization of thiol-Capped CdSe Nanocrystals.

Figure 1d shows XRD patterns obtained from powdered precipitated fractions of CdSe QDs. The QDs belong to the cubic (zinc blende) structure which is also the dominant crystal phase. However, the crystal phase of CdSe QDs (JCPDS Cards No. 19-0191) with slightly broadening toward higher angles (the cubic (zinc blende) CdS phases (JCPDS Cards No. 10-0545)). This is because the synthesis of aqueous colloidal solutions of CdSe QDs needs presence of an excess of thiols (MPA) in basic media. Under these conditions, the partial hydrolysis of thiols leads to incorporate a small amount of sulfur into the growing QDs which resulted in the formation of mixed CdSe(S) QDs under refluxing.¹¹⁻¹³ Combining with the different molar ratio of Cd:MPA:Se (1:1.5:0.25) in our synthetic experiment, above mentioned analysis means the Cd/Se molar ratio of CdSe is not stoichiometric which is consistent with the typical aqueous synthesized QDs in the literature.¹¹⁻¹³

On the other hand, the ICP-OES (Table S4) and XPS (Figure 2, Tables S1-S3) analysis show a considerable amount of sulfur in CdSe QDs. This indicates, besides the incorporated small amount of sulfur as above mentioned, a portion of sulfur serves as surface ligands in the form of MPA. NMR and FT-IR spectral analysis (Figures S6-S7) certified this conclusion, and that the as-synthesized CdSe QDs were capped with a small number of organic thiols-ligands.

3. Control experiment of SILAR method for the synthesis.

An aqueous colloidal CdSe QDs solution with approximately diameters of 1.9 nm were prepared according to the aforementioned procedures.¹⁴ Precursor amounts for each additional monolayers (MLs) of the shell material were determined by the number of the surface atoms of CdSe QDs.¹⁵ The as-prepared CdSe QDs (1.9 nm in diameter, 2.0×10^{-5} M, pH \approx 11, 200 mL of CdSe QDs) were placed in a 500 mL three-necked flask, and degassed with N₂ bubbling for 30 min with rigorous stirring. The reaction mixture was then heated to 50°C for the injection. The calculated amount of Na₂S·9H₂O (50 mL, 5 mM) aqueous solutions for one monolayer was one-off injected into the flask with a speed of 10.0 mL/40 min by syringe pump to produce S-terminated CdSe (CdSe/S) after 2 h of growth. On the other hand, the calculated amount of Cd(ClO₄)₂·6H₂O (50 mL, 5 mM) aqueous solutions for one

monolayer was one-off injected into the CdSe QDs flask with a speed of 10 mL/40 min by syringe pump to produce Cd-terminated CdSe (CdSe/Cd) after 2 h of growth. Further, in the same flask at the same temperature, the calculated amount of Na₂S·9H₂O (50 mL, 5 mM) aqueous solutions for one monolayer was one-off injected into the flask with a speed of 10.0 mL/40 min by syringe pump, then Cd(ClO₄)₂·6H₂O (50 mL, 5 mM) aqueous solution was injected with a speed of 10 mL/40 min by syringe pump to form Cd-terminated CdSe (CdSe/S/Cd) after 2 h of growth. The detailed characterization was given in Figures S2-S5. Other control experiments, such as higher reaction temperature (100°C), were operated under the same condition with corresponding factor changed.

4. Steady state and time-resolved emission spectroscopy measurement.

Steady state and time-resolved emission spectroscopy were recorded using an Edinburgh FLS-920 spectrometer. Unless otherwise specified, a fluorescence quartz cell cuvette with a 10 mm path length was used for measurements. For collection of steady state emission spectra, the excitation wavelength was set to 400 nm, and a 420 nm long-wave pass optical filter was used to remove extraneous wavelengths from the excitation light. Time-resolved emission measurements were made by the time correlate single photon counting (TCSPC) capability of the same instrument (FLS-920). The pulsed excitation light (406 nm, typical pulse width = 86.9 ps) was generated by a Edinburgh EPL-405 ps pulsed laser diode operating at a repetition rate of 1 MHz for CdSe QDs and CdSe/CdS QDs. The maximum emission channel count rate was less than 5% of the laser channel count rate, and each data set collected greater than 5000 counts on the maximum channel with a photomultiplier tube (PMT, R928 Hamamatsu) detector. The lifetime of emission was determined by reconvolution fit with the instrument response function using the Edinburgh F900 software. In all cases, after reconvolution, emission decay was satisfactorily fit with a triple exponential function (Table S5).

5. Femtosecond transient absorption spectroscopy measurement.

The femtosecond transient absorption spectroscopy apparatus with a temporal resolution of ~160 fs is briefly described below: an optical parametric amplifier (OPA-800 CF-1, Spectra Physics) pumped by a regenerative amplifier (SPTF-100F-1KHPR, Spectra Physics) provided the actinic laser pulses at desired wavelengths (~120 fs, full width at half-maximum). A white light continuum probe (430~1400 nm) was generated from a 3 mm thick sapphire plate and was detected after interrogating the excited sample by a CCD detector (Spec-10:400B/LN) for the visible region. To ensure that each laser shot excites the sample relaxed fully from the previous excitation, the laser system was run at a repetition rate of 100 Hz. A mechanical chopper (model 75158, Newport) was set in the

pump beam to regulate pump “on” and “off” for a pair of sequential actinic pulses.

6. Steady state and time-resolved X-ray transient absorption (XTA) measurement.

The steady state X-Ray absorption spectroscopy measurements were performed at Beamline 1W2B of the Beijing Synchrotron Radiation Facility (BSRF) under 2.5 GeV and 250-150 mA, and collected in transmission mode for Nickel standards and in fluorescence mode for QDs samples using a Lytle detector. Energy was calibrated using a nickel foil. The data analysis was carried out by Athena software.¹⁶ Time-resolved X-ray transient absorption (XTA) measurement was performed at 11-ID-D beamline at the Advanced Photon Source (APS) of Argonne National Laboratory. The 400 nm, 100 fs laser pump pulse was the second harmonic output of a Nd:YLF fs Ti:Sapphire regenerative amplified laser operating at 10 kHz repetition rate. The experiment was carried out under a hybrid timing mode where an intense X-ray pulse with 16% of the total average photon flux (16 mA/bunch) was separated in time from other weak X-ray pulses. The intense X-ray pulse with 160 ps FWHM and 271.5 kHz repetition rate was used as the probe. The solution was flowed through a stainless steel tube and formed a free jet of 550 μm in diameter. Two avalanche photodiodes (APDs) positioned at 90° angle on both sides of the incident X-ray beam collected the X-ray fluorescence signals. A soller slits/Co filter combination, which was custom-designed for the specific sample chamber configuration and the distance between the sample and the detector, was inserted between the sample fluid jet and the APD detectors. To mitigate sample radiation damage, the aqueous sample was circulated using a liquid jet under irradiation by both the 400 nm femtosecond laser and the picosecond X-ray pulse. In the meantime, the sample reservoir was bubbled with nitrogen gas. The detailed setup of the XTA instrumentation could be found elsewhere.¹⁷ The data was averaged over multiple scans for better signal to noise ratio, since the Ni(II) concentration is only 0.5 mM.

The electron transfer to Ni(OH)₂ after light absorption was evidenced by Ni K-edge XTA spectroscopy measurement, which allows us to selectively probe the specific metal center to track the electron density change at Ni center during the photoinduced electron transfer process.¹⁸ Due to unexpected coagulation property of CdSe/CdS-Ni(OH)₂ system toward irradiation of laser and X-ray, we used CdSe/ZnS-Ni(OH)₂ system to measure XTA (Note that the CdSe/ZnS QDs, compared to CdSe/CdS QDs, were synthesized at the same concentrations except for the replacement of Cd by Zn). Figure 6b shows XANES spectra of the ground state (blue line, laser-off) of CdSe/ZnS-Ni(OH)₂, and the difference spectra (black line, laser-on subtracting laser-off). The transient signal due to laser excitation was observed in the difference XANES spectrum (black line) after subtracting the laser-off spectrum from the laser-on spectrum. These changes showing a sharp, positive feature at 8.342 keV and a weak,

negative feature at 8.350 keV, express the red-shift of excited state spectra as compared to its ground state ones. Although these changes are small, they are real and reflect the oxidation state change of the Ni center, indicating that the edge of Ni center shifts to lower energy due to photoexcitation of CdSe/ZnS in the CdSe/ZnS-Ni(OH)₂.¹⁹ These results unambiguously determine the electron transfer process from excited CdSe/ZnS to Ni(OH)₂ clusters.

7. XPS sensitivity calibration and surface composition calculation.

To determine the relative composition in XPS, the intensity of a given photoelectron signal has to be corrected for the atomic sensitivity factor, S. In the case of a homogeneous bulk sample this is given as 1/S, where S is proportional to the inelastic mean free path of the photoelectrons. For nanocrystals an additional correction has to be made to this sensitivity factor that accounts for the spherical or elliptical geometry and the small nanocrystal size. We follow a calibration procedure described in the literature²⁰⁻²² to correct the overall Cd/S/Se ratio in the XPS measurement taking consideration of varied inelastic mean free path of the photoelectrons escaped from different atoms. The corrected Cd/S/Se ratios of two QDs samples are shown in Table S1.

To determine the relative percentage of Cd/S/Se on the surface, we assumed spherical geometry for CdSe QDs with a diameter 1.9 nm, and elliptical geometry for CdSe/CdS with a diameter about 2.0 nm and a length around 5.0 nm determined from the statistic HRTEM measurement. In this situation, the overall numbers of Cd, S and Se atoms in the QD were determined using the integrated XPS data (Table S2) for each atom. Next, the relative fraction of surface-to-inner atoms of Cd, S and Se was determined from the ratio of the integrated areas for the surface or core atom curve fits to the raw XPS data (Table S3). Combining the total number of atoms (Cd, S or Se) with the percentage of surface atoms, the relative percentage of Cd, S or Se on the surface could be determined (Table S1).²⁰⁻²²

Table S1. XPS Composition of CdSe QDs and CdSe/CdS QDs on the surface.^[a]

	<i>D/L</i> (nm)	Cd/Se corrected	S/Se corrected	Cd/S corrected	Cd _s /Cd _i ratio	S _s /S _i ratio	Se _s /Se _i ratio	Surface %		
								Cd	S	Se
CdSe	1.9 _D	5.39	4.43	1.22	0.39	0.36	0.67	49.03	37.99	12.98
CdSe/CdS	2.0 _D /5.2 _L	12.20	11.25	1.08	0.29	0.67	0.32	36.58	60.21	3.21

[a] D and L are the diameter and (or) length of the QDs determined from the statistic HRTEM measurement; Cd-S-Se ratios were read from XPS. Surface-to-inner ratio of Cd, S and Se (Cd_s/Cd_i, S_s/S_i and Se_s/Se_i) are calculated from integrated peak area fitted by Cd, S and Se signals in XPS.

Table S2. XPS composition of CdSe QDs and CdSe/CdS QDs, and the atomic percentage of elements in each sample obtained from raw XPS data.^[a]

	<i>D/L</i> (nm)	C%	O%	Cd%	S%	Se%	Cd/Se ratio	S/Se ratio	Cd/S ratio
CdSe	1.9 _D	55.10	24.41	10.53	8.22	1.74	6.05	4.72	1.28
CdSe/CdS	2.0 _D /5.0 _L	42.9	26.28	14.46	13.01	1.15	12.57	11.31	1.11

[a] D and L are the diameter and (or) length of the QDs determined from the statistic HRTEM measurement. Atoms ratio of Cd, S and Se (Cd/Se, Cd/S, and S/Se) are calculated from integrated peak area fitted from Cd, S and Se signals in XPS data.

Table S3. Detailed XPS peak analysis. Raw XPS data was fit with Gaussian functions as shown in Figure 2 in the main text. In each sample, Inn indicates signals from inner atoms of Cd, S or Se (also represented by the blue fitting curves in Figure 2), while Surf. represents contributions to signals from surface atoms (the red fitting curves).

Sample	Peak	Binding Energy (eV)	FWHM	Area	%Conc.	
CdSe	C	1s	284.60	2.3		
	Inn. Cd	3d 5/2	404.91	1.71	108720	71.94
		3d 3/2	411.63	1.55	72842	
	Surf. Cd	3d 5/2	405.7	1.24	42400	28.06
		3d 3/2	412.57	1.2	28408	
	Inn. S	2p 3/2	160.77	1.70	8098	73.53
		2p 1/2	161.97	1.64	4049	
		2p 3/2	162.09	1.67	4290	
	Surf. S	2p 3/2	162.09	1.67	4290	26.47
		2p 1/2	163.29	1.63	2145	
	Inn. Se	3d 5/2	52.96	1.60	2037	59.88
		3d 3/2	53.81	1.38	1365	
Surf. Se		3d 5/2	54.05	0.98	1025	
		3d 3/2	54.9	0.98	687	
CdSe-CdS	C	1s	284.60	2.2		
	Inn. Cd	3d 5/2	404.95	1.58	236881	80.65
		3d 3/2	411.72	1.43	158710	
	Surf. Cd	3d 5/2	405.9	1.12	56851	19.35
		3d 3/2	412.7	1.09	38090	
	Inn. S	2p 3/2	160.85	1.60	13568	60.60

	2p1/2	162.05	1.55	6784	
Surf. S	2p 3/2	161.84	1.39	10013	39.40
	2p1/2	163.04	1.39	5006	
Inn. Se	3d 5/2	53.63	1.45	2654	74.62
	3d 3/2	54.48	1.49	1778	
Surf. Se	3d 5/2	54.54	1.06	642	25.37
	3d 3/2	55.39	1.01	430	

8. Table S4

Table S4. The wt.% composition of CdSe QDs and CdSe/CdS QDs determined by ICP-OES measurement.

wt.%	Cd	Se	S	Ni
CdSe	46.39	12.66	8.09	0.00
CdSe-Ni(OH) ₂	44.84	12.03	7.15	6.19
CdSe/CdS	56.18	4.24	12.35	0.00
CdSe/CdS-Ni(OH) ₂	54.54	3.83	11.68	6.79

According to the ICP-OES measurement, the number of nickel atom units on one CdSe/CdS QDs was calculated. And nickel adsorption on the CdSe/CdS QDs surface was 6.8 wt.% (corresponding to nearly 70% nickel). Thus, the average number of nickel units per CdSe/CdS QDs was estimated to be approximate 23. For comparison, the number of nickel atom units on one CdSe QDs was controlled almost the same as CdSe/CdS QDs.

9. The internal quantum efficiency (IQE) determination.

In order to determine the internal quantum efficiency, the amount of absorbed light was determined from reaction solution absorbance (abs) at the incident wavelength. Because the scattering loss of the suspension is not taken into account, the estimated internal quantum yield should be taken as the lower limit. Light-driven H₂ production was performed in a standard spectro-cell with a total volume of ~4 mL and a path-length of 1 cm. The cuvette was filled with 3.0 mL solution of IPA and water (IPA:H₂O = 1:1, v:v = 1:1 at pH 10 ± 0.2), containing NiCl₂·6H₂O (2.1 × 10⁻⁴ M), CdSe/CdS QDs (6.5 × 10⁻⁶ M). The internal quantum efficiency (IQE) was measured using monochromatic LED light source (λ = 455 nm, light intensity 160 mW cm⁻² at spectro-cell surface) with constant stirring by a magnetic stirrer, and calculated by using the following equation:

$$IQE(\%) = \frac{2 \times \text{Number of photogenerated H}_2 \text{ molecules}}{\text{Number of absorbed photons}} \times 100 \quad (5)$$

Where the number of photogenerated H₂ were obtained from drainage gas-collecting method using a gas-tight acid burette, and the number of absorbed photons were calculated from the illumination power and absorbance of the reaction solution. The illumination power was measured using a digital photodiode power meter. The amount of absorbed light was determined from reaction solution absorbance (abs) at the illuminated wavelength. From the combined measurements of H₂ mass production and the specific light absorption, the quantum yield was measured as ~52 % at 455 nm.

10. The turnover number (TON) determination.

Turnover number (TON) is usually defined by the number of H₂ molecules generated by light to that of the number of individual molecules of CdSe/CdS QDs, and then it is determined using the following equations:

$$TON = \frac{\text{Number of photogenerated H}_2 \text{ molecules}}{\text{Number of CdSe/CdS nanorods}} \quad (6)$$

where the number of H₂ molecules generated by light is determined by drainage gas-collecting method using a gas-tight acid burette. The number of individual CdSe/CdS QDs is obtained by counting the initial number of CdSe/CdS QDs added in the reaction system.

11. Measured and estimated time constants of recovery kinetics of emission delay.

The band edge emission decays of CdSe/CdS QDs in the absence and presence of Ni²⁺ ions or IPA were studied and the decay traces for the samples were well fitted with triplet-exponential function $Y(t)$ based on nonlinear least-squares, using the following expression.^{23,24}

$$Y(t) = B_1 \exp(-t/\tau_1) + B_2 \exp(-t/\tau_2) + B_3 \exp(-t/\tau_3) \quad (7)$$

where B_1 , B_2 , B_3 are fractional contributions of time-resolved emission decay lifetimes τ_1 , τ_2 , τ_3 and the average lifetime τ could be concluded from the equation (8).^{23,24}

$$\langle \tau \rangle = \frac{B_1 \tau_1^2 + B_2 \tau_2^2 + B_3 \tau_3^2}{B_1 \tau_1 + B_2 \tau_2 + B_3 \tau_3} \quad (8)$$

Table S5. Measured and estimated the time constants of recovery kinetics from emission delay at 495 nm.

	τ_1 (ns)	B_1	τ_2 (ns)	B_2	τ_3 (ns)	B_3	χ^2	average life-time(ns)
CdSe/CdS	0.723	2.88E-01	7.19	6.95E-02	30.7	1.53E-02	1.269	15.4

CdSe/CdS-Ni(OH) ₂	0.431	1.17E-01	3.14	1.34E-02	57.7	7.42E-03	1.208	2.96
CdSe/CdS-IPA	0.405	2.92E-01	3.75	1.25E-02	18.3	2.08E-03	1.255	4.54

12. The kinetics of the excited QD population ($N_{QD^*}(t)$)

If the charge separation kinetics are not single-exponential, the kinetics of QD excited state can be fit according to the following equation, developed by Lian *et.al.*²⁵:

$$N_{QD^*}(t) = \sum_i A_i e^{-k_{CS,i}t} - e^{-k_0 t} \quad (9)$$

Here, $1/k_0$ (~ 1.38 ps) is the formation time of the 1S exciton bleaching. This rise time reflects the cooling of the conduction band electrons to the 1S(e) level, similar to those in the free QDs. Satisfactory fits to the QD decay kinetics can be obtained using triexponential functions with amplitudes and time constants of A_i and $k_{CS,i}$, respectively. The fitting parameters are listed in Table S6.

According to equation (9), the population of the charge separated state increases with the rate of the charge separation process and decays with the rate of charge recombination. We used the $1/e$ time for the QD excited state decay ($N_{QD^*}(t)$) to represent the average charge separation times using amplitudes and time constants of A_i and $k_{CS,i}$, respectively. This means the time t is the average lifetime when the $N_{QD^*}(t)$ is equal to the $1/e$ of $N_{QD^*}(0)$. According to this equation, the average time is approximate 9 ns and 1.4 ns for CdSe/CdS QD and hybrid CdSe/CdS-Ni(OH)₂ photocatalyst, respectively.

Table S6. Fitting parameters for the decay kinetics of CdSe/CdS QD and CdSe/CdS-Ni(OH)₂ photocatalyst according to equation (9).

Sample	k_0, ps^{-1}	k_1, ps^{-1} (A1, %)	k_2, ps^{-1} (A2, %)	k_3, ps^{-1} (A3, %)	1/e life (ps)
CdSe/CdS	0.725	1.107×10^{-4} (100)	0	0	9030
Sample	k_0, ps^{-1}	$k_{CS,1}, \text{ps}^{-1}$ (A1, %)	$k_{CS,2}, \text{ps}^{-1}$ (A2, %)	$k_{CS,3}, \text{ps}^{-1}$ (A3, %)	1/e life (ps)
CdSe/CdS-Ni(OH) ₂	0.725	1.53 (21.9)	0.024 (17.4)	2.675×10^{-4} (60.7)	1390

13. Figure S1.

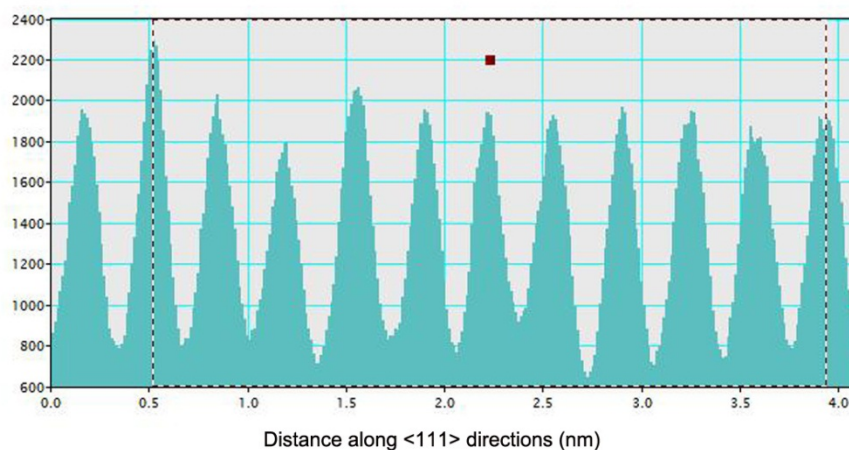


Figure S1 The corresponding lattice spacing along the crystalline $\langle 111 \rangle$ directions of the zinc blende lattice in CdSe/CdS QDs, and the lattice spacing is 3.42 \AA obtained from average of the ten distances.

14. Figure S2 - Figure S5.

Figure S2.

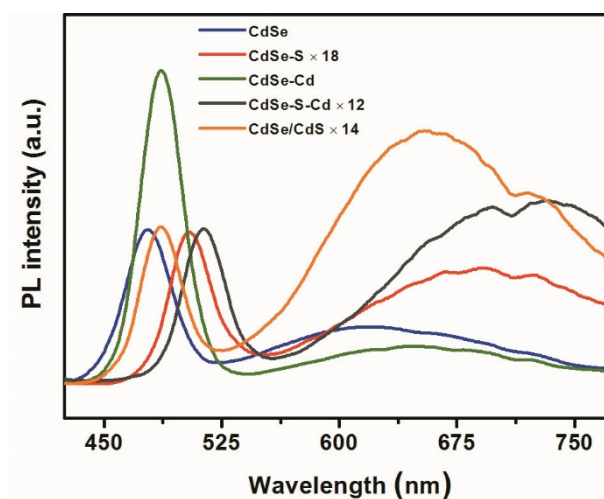


Figure S2 Emission spectra for CdSe QDs (blue), CdSe QDs with one monolayer of S added (red), CdSe QDs with one monolayer of Cd added (green), CdSe QDs with one monolayer of S added and an additional layer of Cd added (black), and as prepared CdSe/CdS QDs (orange). Spectra were acquired for the same relative absorbance so that relative emission efficiency can be compared. Note that partial spectral intensity was multiplied by a certain ratio for comparison.

Figure S3.



Figure S3 Images of CdSe QDs solution, CdSe QDs with one monolayer of S added, CdSe QDs with one monolayer of Cd added, CdSe QDs with one monolayer of S added and an additional layer of Cd added, and as prepared CdSe/CdS QDs.

Figure S4.

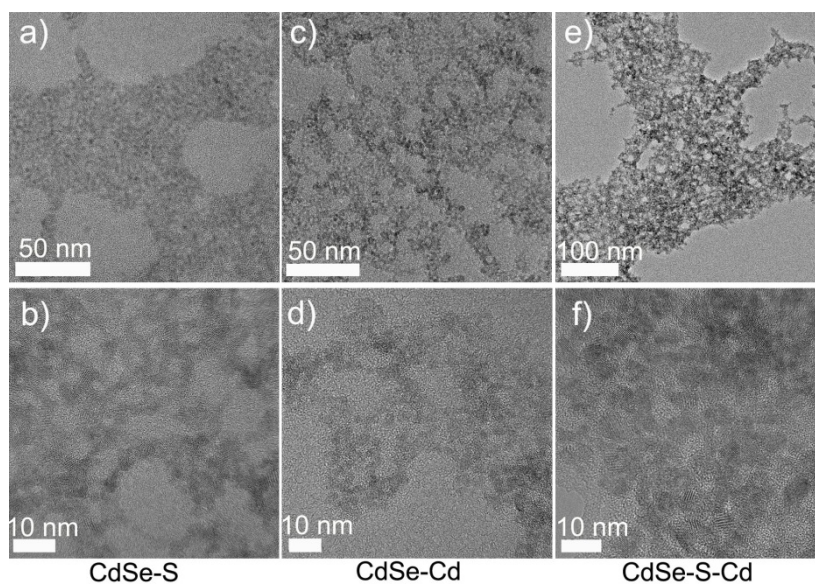


Figure S4 HRTEM images of the CdSe QDs with one monolayer of S added (a-b), CdSe QDs with one monolayer of Cd added (c-d), CdSe QDs with one monolayer of S added and an additional layer of Cd added (e-f).

Figure S5.

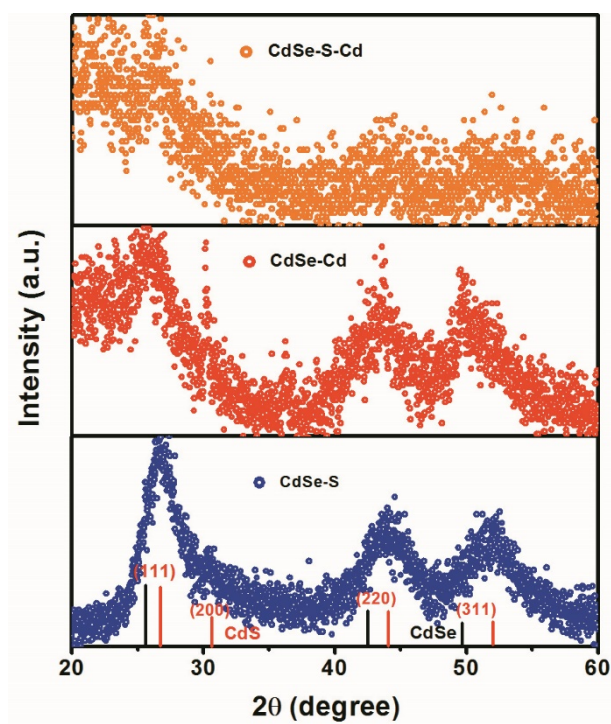


Figure S5 XRD patterns of the CdSe QDs with one monolayer of S added (bottom), CdSe QDs with one monolayer of Cd added (middle), CdSe QDs with one monolayer of S added and an additional layer of Cd added (top).

15. Figure S6.

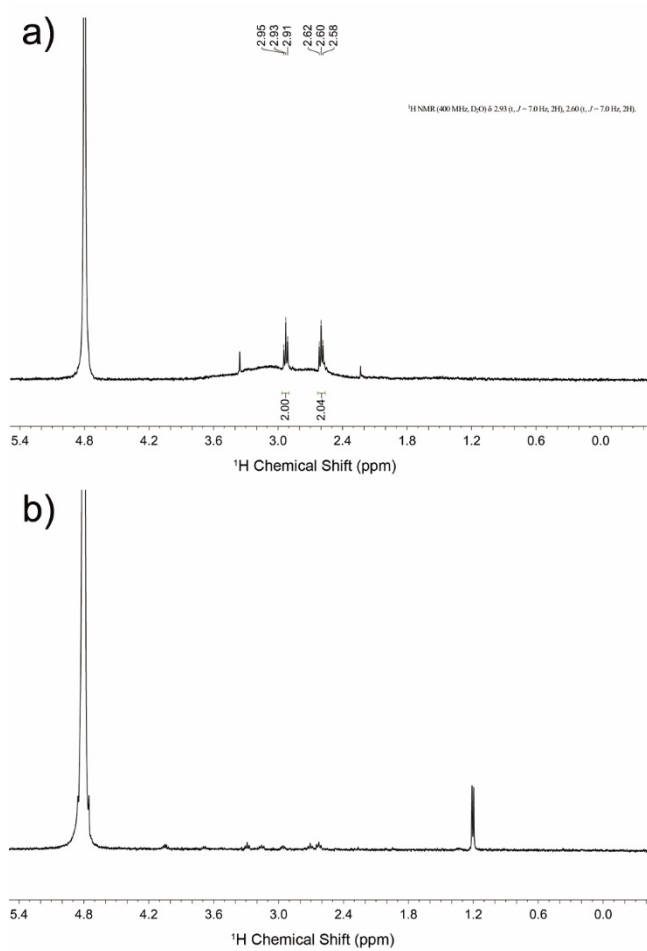


Figure S6 ^1H NMR spectra of MPA obtained from CdSe QDs and the CdSe/CdS QDs in D_2O .

16. Figure S7.

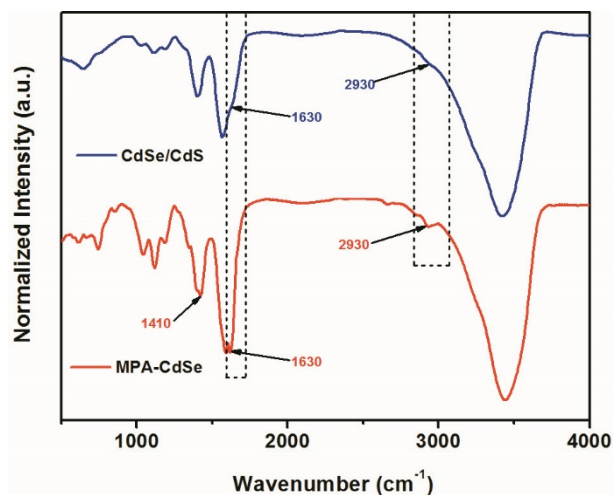


Figure S7 Room temperature FT-IR spectra of MPA-CdSe QDs and CdSe/CdS QDs.

A featuring peak at $2,930\text{ cm}^{-1}$ corresponding to the $\text{CH}_2\text{-S}$ bonding²⁶ was clearly observed in the FT-IR spectrum, which suggested the existence of MPA molecules on the surface of MPA-CdSe QDs. MPA molecules also show strong C=O asymmetric vibration at 1630 cm^{-1} and symmetric vibration at $1,410\text{ cm}^{-1}$ for COO^- group in MPA-CdSe QDs.^{27, 28} These peaks were noted too weak to be detected in the FT-IR spectrum of CdSe/CdS QDs, implying that the MPA molecules were hardly existed on the surface of CdSe/CdS QDs. From the above results, the CdSe/CdS QDs studied in this work could be identified as an all-inorganic surface composition.

17. Figure S8.

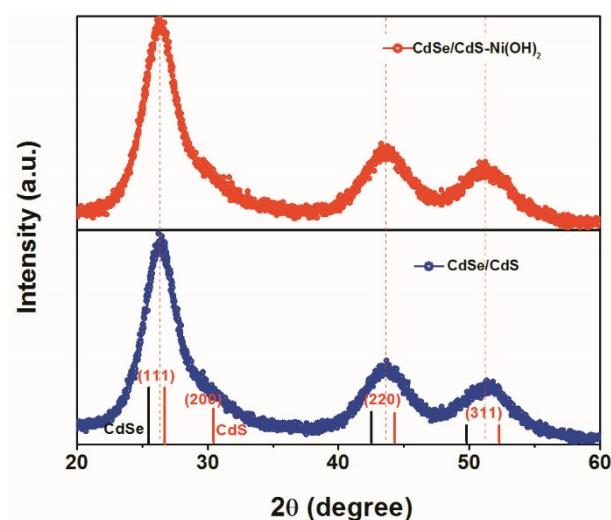


Figure S8 XRD patterns of the CdSe/CdS QD and CdSe/CdS-Ni(OH)₂ photocatalyst.

18. Figure S9.

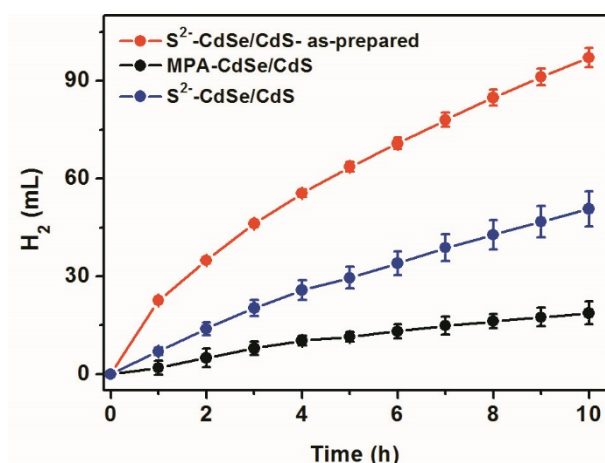


Figure S9 Comparison of photocatalytic H₂-production performance of as-prepared CdSe/CdS QDs (red line) with CdSe/CdS QDs (blue and blank lines) prepared by organometallic route in 5 mL solution of IPA and water (IPA:H₂O = 1:1 (v:v), pH ≈ 10), containing of NiCl₂·6H₂O (2.1×10^{-4} M) under visible light irradiation for 10 h ($\lambda \approx 455$ nm). The organic phase synthesized CdSe/CdS QDs were prepared using previously published methods,²⁹ and then transformed into water by ligand exchange with 3-mercaptopropionic acid (MPA)²⁹ and inorganic S²⁻ ligands.³⁰ The CdSe/CdS QDs concentrations were adjusted to ensure that all solutions had the same absorbance at the illumination wavelength, so that the relative efficiency can be compared. Error bars represent mean ± s.d. of three independent experiments.

19. Figure S10.

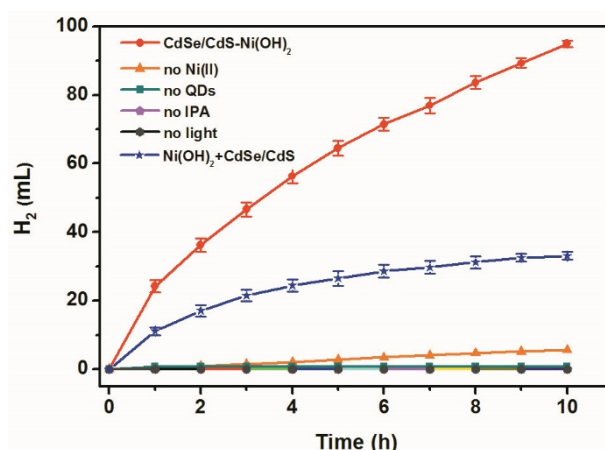


Figure S10 Photocatalytic H₂ evolution in 5 mL solution of IPA and water (IPA:H₂O = 1:1 (v:v), pH ≈ 10), containing of NiCl₂·6H₂O (2.1×10^{-4} M), CdSe/CdS QDs (6.5×10^{-6} M), under visible light irradiation for 10 h ($\lambda \approx 455$ nm) (solid circle). Control experiments were operated at the same concentration and conditions with one

component absent or being substituted (triangle: the sample without $\text{NiCl}_2 \cdot 6\text{H}_2\text{O}$; cubic: the sample without CdSe/CdS QDs; pentagon: the sample without IPA; hexagon: the sample without light irradiation; star: CdSe/CdS QD was added into established $\text{Ni}(\text{OH})_2$ precipitate which prepared by directly adding $\text{NiCl}_2 \cdot 6\text{H}_2\text{O}$ to pure water ($\text{pH} \approx 10$) with rigorous stirring; Error bars represent mean \pm s.d. of three independent experiments.

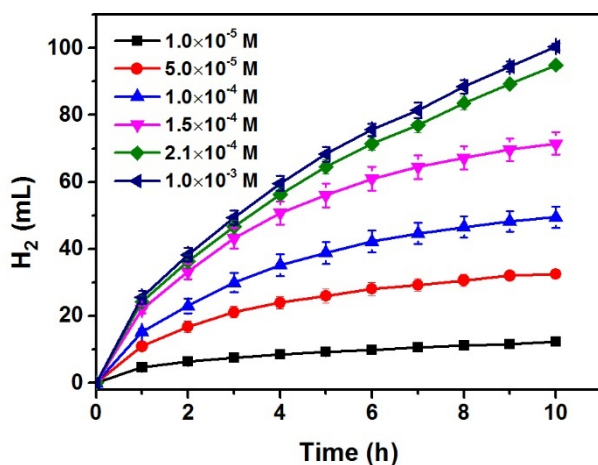


Figure S11 Photocatalytic H_2 evolution in 5 mL solution of IPA and water (IPA: H_2O = 1:1 (v:v), $\text{pH} \approx 10$), containing CdSe/CdS QDs (6.5×10^{-6} M), and various concentrations of $\text{NiCl}_2 \cdot 6\text{H}_2\text{O}$ under visible light irradiation for 10 h ($\lambda \approx 455$ nm).

20. **Figure S12.**

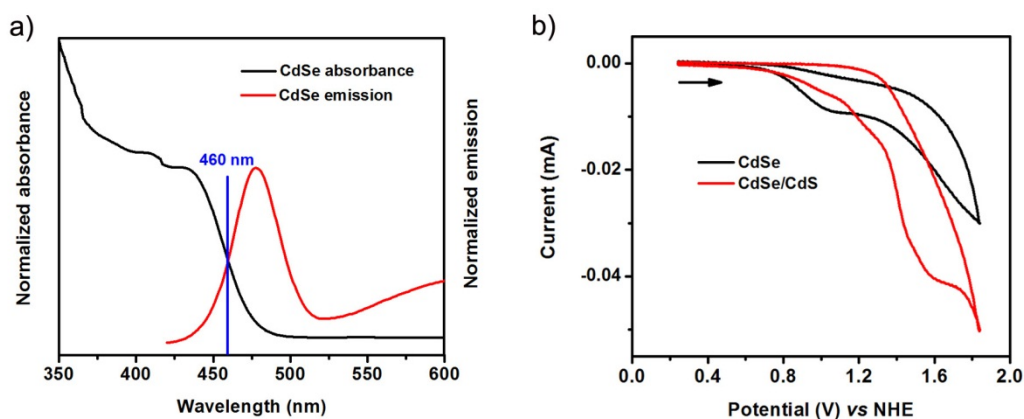


Figure S12 (a) Normalized absorption (black) and emission (red) spectra of CdSe QDs. (b) Cyclic voltammogram of 2.0×10^{-4} M CdSe QDs (black) and 1.3×10^{-4} M CdSe/CdS QDs (red) solution in water-no electrolyte, 100 mV s^{-1} .

21. **Figure S13.**

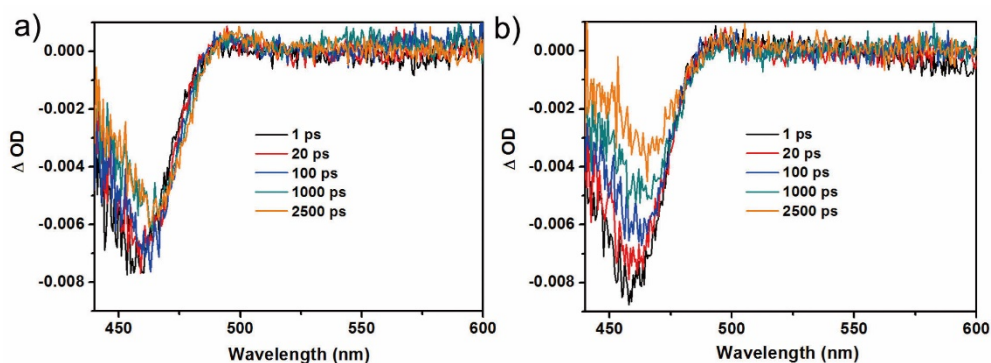


Figure S13 The femtosecond TA spectra of CdSe/CdS QDs in the absence (a) and presence (b) of Ni(II) monitored at 460 nm at indicated delay times (1~2500 ps) after laser-pulsed excitation at 400 nm. In aqueous QDs synthesis, the internal and surface defect states affect much seriously than QDs synthesis in organometallic route. So the bleaching for CdSe/CdS QDs in TA spectrum is hard to recover completely even on a long time scale, as existed of these bound states of electrons or holes. But, this tailing factor beyond 2.5 ns might not influence the the initial charge separation from excited CdSe/CdS to Ni(OH)₂ clusters because the initial bleaching recover is quickly.

22. Figure S14.

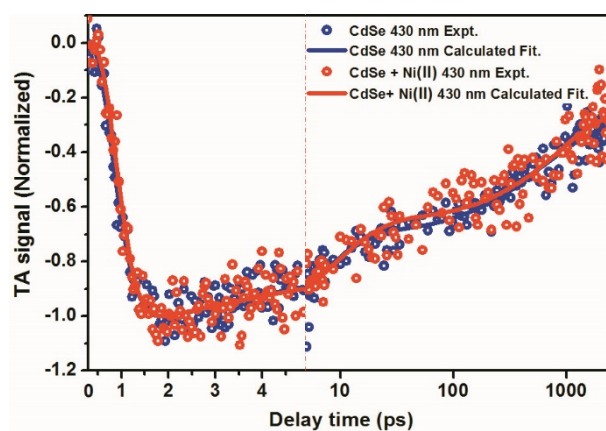


Figure S14 The femtosecond recovery kinetics of CdSe QDs bleaching in the absence and presence of Ni(II) monitored at 430 nm (the x-axis is in linear scale from 0 to 5 ps and in logarithmic scale from 5 ps to 2500 ps); The recovery kinetics of transient bleaching for MPA-CdSe QDs and CdSe QDs with Ni(II) normalized at the maximal signal.

23. References

1. Z.-J. Li, J.-J. Wang, X.-B. Li, X.-B. Fan, Q.-Y. Meng, K. Feng, B. Chen, C.-H. Tung and L.-Z. Wu, *Adv. Mater.*, 2013, **25**, 6613-6618.
2. W. W. Yu, L. Qu, W. Guo and X. Peng, *Chem. Mater.*, 2003, **15**, 2854-2860.
3. A. M. Smith and S. Nie, *Acc. Chem. Res.*, 2009, **43**, 190-200.
4. D. J. Norris and M. G. Bawendi, *Phys. Rev. B*, 1996, **53**, 16338-16346.
5. A. Kudo and Y. Miseki, *Chem. Soc. Rev.*, 2009, **38**, 253-278.
6. M. N. Kalasad, M. K. Rabinal and B. G. Mulimani, *Langmuir*, 2009, **25**, 12729-12735.
7. S. Sapra and D. D. Sarma, *Phys. Rev. B*, 2004, **69**, 125304.
8. H. Chen, C. Chen, Y. C. Chang, C. W. Tsai, R. S. Liu, S. F. Hu, W. S. Chang and K. H. Chen, *Angew. Chem. Int. Ed.*, 2010, **49**, 5966-5969.
9. M. Amelia, C. Lincheneau, S. Silvi and A. Credi, *Chem. Soc. Rev.*, 2012, **41**, 5728-5743.
10. H. Zhu, N. Song and T. Lian, *J. Am. Chem. Soc.*, 2011, **133**, 8762-8771.
11. N. Gaponik, D. V. Talapin, A. L. Rogach, K. Hoppe, E. V. Shevchenko, A. Kornowski, A. Eychmüller and H. Weller, *J. Phys. Chem. B*, 2002, **106**, 7177-7185.
12. H. Zhang, Z. Zhou, B. Yang and M. Gao, *J. Phys. Chem. B*, 2002, **107**, 8-13.
13. A. L. Rogach, "*Mater. Sci. Eng., B*", 2000, **69-70**, 435-440.
14. R. D. L. Smith, M. S. Prévot, R. D. Fagan, Z. Zhang, P. A. Sedach, M. K. J. Siu, S. Trudel and C. P. Berlinguette, *Science*, 2013, **340**, 60-63.
15. P. Reiss, M. Protière and L. Li, *Small*, 2009, **5**, 154-168.
16. B. Ravel and M. Newville, *J. Synchrotron Rad.*, 2005, **12**, 537-541.
17. L. X. Chen and X. Zhang, *J. Phys. Chem. Lett.*, 2013, **4**, 4000-4013.
18. G. Smolentsev and V. Sundström, *Coord. Chem. Rev.*, 2015, **304**, 117-132.
19. Y. Tang, B. Pattengale, J. Ludwig, A. Atifi, A. V. Zinovev, B. Dong, Q. Kong, X. Zuo, X. Zhang and J. Huang, *Sci. Rep.*, 2015, **5**, 18505.
20. S. K. Kulkarni, U. Winkler, N. Deshmukh, P. H. Borse, R. Fink and E. Umbach, *Appl. Surf. Sci.*, 2001, **169-170**, 438-446.
21. J. Jasieniak and P. Mulvaney, *J. Am. Chem. Soc.*, 2007, **129**, 2841-2848.
22. H. H.-Y. Wei, C. M. Evans, B. D. Swartz, A. J. Neukirch, J. Young, O. V. Prezhdo and T. D. Krauss, *Nano Lett.*, 2012, **12**, 4465-4471.
23. S. N. Sharma, Z. S. Pillai and P. V. Kamat, *J. Phys. Chem. B*, 2003, **107**, 10088-10093.
24. C. Higgins, M. Lunz, A. L. Bradley, V. A. Gerard, S. Byrne, k. Gun, Yurii K., V. Lesnyak and N. Gaponik, *Opt. Express* 2010, **18**, 24486-24494.
25. H. Zhu, N. Song and T. Lian, *J. Am. Chem. Soc.*, 2010, **132**, 15038-15045.
26. A. C. A. Silva, S. W. da Silva, P. C. Morais and N. O. Dantas, *ACS Nano*, 2014, **8**, 1913-1922.

27. C. Dong, H. Qian, N. Fang and J. Ren, *J. Phys. Chem. B*, 2006, **110**, 11069-11075.
28. H. Chen, R. Li, L. Lin, G. Guo and J.-M. Lin, *Talanta*, 2010, **81**, 1688-1696.
29. H. Zhu, N. Song, H. Lv, C. L. Hill and T. Lian, *J. Am. Chem. Soc.* , 2012, **134**, 11701-11708.
30. A. Nag, D. S. Chung, D. S. Dolzhenkov, N. M. Dimitrijevic, S. Chattopadhyay, T. Shibata and D. V. Talapin, *J. Am. Chem. Soc.* , 2012, **134**, 13604-13615.